

Multiscale Simulation for Conducting Conjugated Polymers from Solution to the Quenching State

Cheng K. Lee,[†] Chi C. Hua,^{*,†} and Show A. Chen[‡]

Department of Chemical Engineering, National Chung Cheng University, Chia-Yi 621, Taiwan, R.O.C and Department of Chemical Engineering, National Tsing Hua University, Hsin-Chu 30013, Taiwan, R.O.C

Received: July 31, 2009; Revised Manuscript Received: October 20, 2009

Innovation in modern material science exploiting conducting conjugated polymers imperatively demands fundamental knowledge of single-chain conformations from solution to the quenching state. This urgent goal, however, poses a stringent challenge to existing simulation schemes, especially when the polymer of interest possesses simultaneously a high molecular weight and anisotropic local interaction forces, such as hydrogen-bond (HB) and $\pi-\pi$ interactions. Considering a standard case with polyaniline emeraldine base (PANI-EB), widely used as the conducting layer in polymer-based optoelectronic devices, this paper introduces how the current difficulty may be circumvented by using a multiscale simulation scheme that takes advantage of a systematic mapping and back-mapping between atomistic molecular dynamics (AMD), coarse-grained molecular dynamics, and coarse-grained Langevin dynamics (CGLD). Whereas a self-consistent CGLD simulation greatly facilitates reaching representative long-chain conformations in specific solvents, the back-mapped AMD simulation permits scrutiny into the effects of localized HB and $\pi-\pi$ interactions on quenched chain morphologies. The basic idea behind this multiphase simulation scheme for conducting conjugated polymers has been consolidated by the central observation for PANI-EB: whereas segmental van der Waals interactions dominate fundamental single-chain properties in solution (i.e., persistence length, solvent quality, and chain diffusivity), the anisotropic HB and $\pi-\pi$ interactions accordingly “trap” the quenched chain to a morphology closely mimicking that in the prior solution state—the first microscopic evidence of the so-called “memory effect.” Notably, the central features disclosed for PANI-EB as well as the multiscale simulation strategy proposed for tracking single-chain conformations from solution to the quenching state are asserted to hold for typical conducting conjugated polymers that possess, ubiquitously, a semiflexible backbone and localized interaction forces.

1. Introduction

Over the past two decades, semiconducting conjugated polymers, which provide flexibility as polymers as well as conductivity as metals, have been the subject of extensive research exploring novel solution-processable optoelectronic materials. Polyaniline (PANI) is among the most widely studied conjugated polymers because of its ease in synthesis, low cost, and high conductivity.¹ To date, PANI has found widespread applications ranging from antistatic and anticorrosion coatings to chemical sensors, electrodes, capacitors, and batteries. There are mainly three types of PANI: LEB, EB, and PNB,^{1,2} as sketched in Figure 1. PANI-EB and its salt derivatives have the best conductivity among them and are often used as a conducting layer in polymer-based light emitting diodes (PLED).^{2,3} In practical processing, however, PANI-EB is difficult to disperse, even in the most commonly used solvent, *n*-methyl-2-pyrrolidinone (NMP).⁴ Moreover, interchain hydrogen bonds prevail in PANI-EB solutions⁵ and are often believed to give rise to gelation under a short-term storage.^{5,6} Given that the chain conformation in solution has been suggested to greatly impact the conductivity of a polymer thin film,⁷ it appears crucial to gain a comprehensive understanding into elementary single-chain properties of PANI-EB in solution—practically inacces-

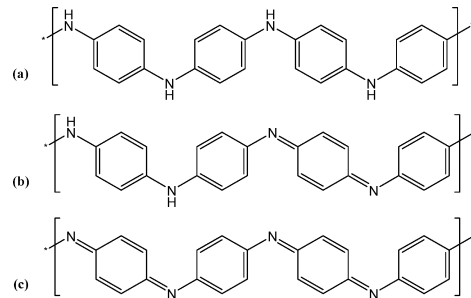


Figure 1. Three different types of polyaniline: (a) leucoemeraldine base (LEB), (b) half-oxidized emeraldine base (EB), and (c) fully oxidized pernigraniline base (PNB).

sible due to the highly aggregated nature of the polymer chain—and, in particular, the way by which solution-state chain conformations impact the subsequent quenching ones in thin film. In principle, the associated aggregation properties may be understood on a similar ground.

The situation depicted above for PANI-EB, in fact, represents some typical challenges in the current applications and future innovations of polymer-based optoelectronic materials. Concretely, the effects of a specific solvent seem enormous in dictating the single-chain and aggregation properties in the precursor solution, and in particular, how and to what extent these solution properties would be carried into a dried thin film—the so-called “memory effect”⁸—remain elusive at a

* Corresponding author. Phone: 886-5-2720411, ext 33412. Fax: 886-5-2721206. E-mail: chmcch@ccu.edu.tw.

[†] National Chung Cheng University.

[‡] National Tsing Hua University.

microscopic level. At first sight, computer simulations may help reveal essential insights into these perspectives. The major challenge is, however, to compromise the two different needs of producing representative (well-equilibrated) long-chain conformations in specific solvents and, on the other hand, capturing the detailed structure sensitive to local interaction forces, such as the $\pi-\pi$ interactions that are ubiquitous in conjugated polymer chains. The following historic perspectives help outline the current situation and major challenges to be overcome.

Using polymer models coarse-grained at a level of bead–spring chains as well as mean-field HB forces (if present), early simulations have systematically explored the collapsed single-chain dynamics for understanding the DNA folding,^{9–14} the crystallization process of polymer chains,¹⁵ or the way polymer chain collapses under a sudden variation in solvent quality.¹⁶ Although these simulations were capable of revealing essential insights of long, collapsed chains in solution or after quenching, they have found limited applications with conducting conjugated polymers. The reasons are the model polymer chains employed typically did not capture the effects of a specific solvent, and the length scales considered were too coarse to capture the conformational properties relevant to understanding the optoelectronic properties of a conjugated polymer. On the other hand, most of the prevailing CG polymer models^{17–38} built at finer molecular scales usually have difficulties in simulating long polymer chains in specific solvents, and to our knowledge, no precise CG polymer models have been invented to tackle the effects of anisotropic local interactions, such as HB and $\pi-\pi$ interactions.

To partially resolve the challenges noted above in simulating conjugated polymer solutions, we have recently proposed a self-consistent Langevin dynamics for CG polymer chains that is especially robust for studying single-chain and aggregation properties in specific solvents.³⁷ Since, however, the polymer model still relied on mean-field isotropic interaction forces, it cannot be applied directly to the cases when anisotropic local interactions play an important role, such as in dense or condensed systems. To circumvent this obstacle for the current applications with conducting conjugated polymers, we introduce in this paper a multiscale simulation scheme that takes special advantage of a systematic mapping and back-mapping between atomistic molecular dynamics (AMD), coarse-grained molecular dynamics (CGMD), and coarse-grained Langevin dynamics (CGLD). Whereas the self-consistent CGLD simulation greatly facilitates obtaining representative long-chain conformations in specific solvents, the subsequently back-mapped AMD simulation permits scrutiny into the effects of localized HB and $\pi-\pi$ interactions on the quenching morphologies. The basic idea behind this multiphase simulation scheme for conducting conjugated polymers has been consolidated by the central observation for PANI-EB: whereas segmental van der Waals (vdW) interactions dominate fundamental single-chain properties in solution (i.e., persistence length, solvent quality, and chain diffusivity), the HB and $\pi-\pi$ interactions accordingly dictate the eventual morphologies of the quenched chain. Notably, this essential feature disclosed for PANI-EB chains is asserted to hold for most conducting conjugated polymers that possess ubiquitously a semiflexible backbone and localized interaction forces. In this way, the outcome of a systematic mapping and back-mapping between AMD and CGLD simulations is promising for gaining a closer grasp of the fundamental aspects of conjugated polymer solutions and films.

This article is organized as follows: Section 2 introduces the detailed procedures of constructing the polymer models of

PANI-EB from AMD, CGMD, to CGLD levels, along with a benchmark AMD simulation and some detailed analysis of a 10-mer PANI-EB in NMP, performed to discriminate competing interaction forces affecting static and dynamic single-chain properties in solution. Section 3 reports fundamental single-chain properties of PANI-EB/NMP solution evaluated from the CGMD or CGLD simulations, along with some preliminary results on interchain aggregation. Section 4 discusses the back-mapped AMD simulation for studying the quenching morphologies of PANI-EB, where HB and $\pi-\pi$ interactions are activated for a few well-equilibrated chains to evidence the empirical memory effect. Section 5 remarks on the central implication of this study and a recommendation of future applications.

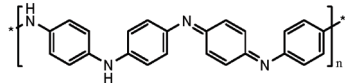
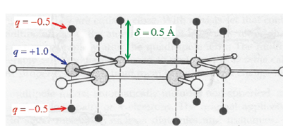
2. System Description and Construction of Coarse-Grained Model

2.1. AMD Simulation. Atomistic molecular dynamics (AMD) simulations have been employed extensively to study the microscopic dynamics and structures of relatively small molecular systems.^{39,40} Through proper time or ensemble averages of atomistic realizations, the crux of macroscopic phenomena may be disclosed. The basic principle of AMD simulations is to follow Newton's equations of motion for all constituent atoms with known interatomic force laws. In contemporary CG simulation schemes developed for long-chain molecules, an AMD simulation typically serves as the starting point in the construction of a hierarchy of more coarse-grained polymer models to properly extend the computationally accessible length and time scales. In this study, a commercial AMD software package, DL_POLY_2,⁴¹ was used along with the force fields provided by DREIDING.⁴² For the purpose of collecting essential statistical trajectories to rebuild the intramolecular forces in the CG polymer model introduced momentarily, AMD simulation of an isolated 10-mer PANI-EB was performed. The Nosé–Hoover *NVT* ensemble (at 298 K) and periodic boundary condition were utilized with a time step size of 1 fs and a cutoff distance 20 Å. Table 1 compiles the chemical structures of the simulated species along with the potential functions employed in the AMD simulation.

To date, the effects of localized, anisotropic HB and $\pi-\pi$ interactions can be treated realistically only in full-atom AMD simulations or first-principles computations. For instance, Karimi-Varzaneh and co-workers³⁶ have recently shown for a molten flexible polymer that, although explicit HB forces were crucial for predicting dynamic and thermal properties, the bulk structural feature can be reasonably captured by a CG polymer model lumping the hydrogen bonds into the usual vdW forces. A similar examination will be performed on the predicted geometric and dynamic properties of PANI-EB in solution after we finish introducing the CG polymer model in the following subsection.

2.2. Construction of CGMD Model. Construction of a CG polymer model can be achieved in a systematic way through essential AMD data defining the new bond lengths and angles in the CG polymer model. By doing so, the corresponding CG simulation captures the minimum molecular details essential for a specific application by saving a lot of computational expense for keeping track of uninterested atomic motions. In the present CGMD simulation, the solvent molecules are treated as single CG particles. Figure 2 depicts how each PANI-EB monomer is represented by four CG particles. These CG particles are all centered at the nitrogen atoms, where particles A and B represent the reduction (with amine nitrogen) and oxidation (with imine

TABLE 1: Molecular Species and Potential Functions Used in the AMD Simulation

Species	Molecular structures
Polymer: PANI-EB	
Solvent: NMP	
Intramolecular potentials	Notation
Bond	$U_{\text{bond}} = \frac{1}{2} k_b (r_{ij} - r_0)^2$ k_b : force constant r_0 : equilibrium bond length
Bond angle	$U_{\text{angle}} = \frac{1}{2} k_\theta [\cos(\theta_{ijk}) - \cos(\theta_0)]^2$ k_θ : force constant θ_0 : equilibrium bond angle
Dihedral angle	$U_{\text{dihed}} = k_d [1 + \cos(m\phi_{ijk} - \delta)]$ k_d : force constant m : periodicity δ : equilibrium dihedral angle
Inversion angle	$U_{\text{inv}} = k_i [1 - \cos(\phi_{ijk})]$ k_i : force constant
Intermolecular potentials	
Van der Waals	$U_{\text{vdw}} = [(A/r_{ij}^{12}) - (B/r_{ij}^6)]$ A, B : van der Waals parameters
Hydrogen bond ^a	$U_{\text{hb}} = D_{\text{hb}} \cos^4(\theta_{jk}) \left[5 \left(\frac{R_{\text{hb}}}{r_{jk}} \right)^{12} - 6 \left(\frac{R_{\text{hb}}}{r_{jk}} \right)^{10} \right]$ D_{hb} : force constant R_{hb} : equilibrium hydrogen bond length
Electrostatic pi-pi interactions ⁴⁶	$U_{\text{elec}} = \frac{1}{4\pi\epsilon_0} \frac{q_i q_j}{r_{ij}}$  q_i, q_j : charge on atom labeled i and j ϵ_0 : permittivity of vacuum

^a For a qualitative purpose, the parameter values for water molecules were employed in all cases: $D_{\text{hb}} = 7.00$ (kcal mol⁻¹) and $R_{\text{hb}} = 2.75$ (Å).^{42,45}

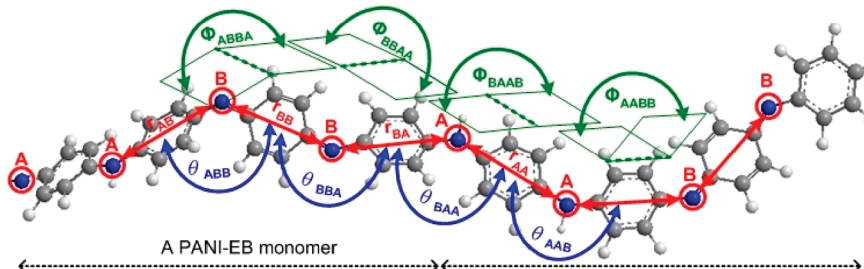


Figure 2. Specifications of the bond lengths and angles for the CG model of a PANI-EB oligomer, where A and B denote the reduction and oxidation states, respectively. The chain conformation depicted here has been obtained from a real AMD simulation corresponding to the most probable states of the bond lengths and angles shown in Figure 3.

nitrogen) states of the monomer, respectively. The present positioning of the CG particles has the obvious advantages of capturing chain flexibility and, on the other hand, facilitating the allocation of hydrogen bonds in a later back-mapping procedure.

Figure 3 shows the distribution functions obtained from AMD simulations that have been corrected for the Jacobian factors associated with the two major types of bond angles. The underlying intramolecular potential functions can, in principle, be constructed from the Boltzmann inversion $U(z) = -k_B T \ln P(z)$ by assuming independence of all variables z ,^{29,37} where $k_B T$ is the Boltzmann constant times the absolute temperature, and $P(z)$ is the distribution function of the variable z (i.e., bond lengths or angles) defined in the CG polymer model. The

potential functions so obtained were fitted to analytic forms using automatic simplex optimizations and were later employed to recompute the distribution functions for consistency check with AMD simulations. The functional forms utilized and the model parameters so obtained are compiled in Tables 2 and 3, respectively, for the CG model.

For the simplex optimizations of the intramolecular potentials listed in Tables 2 and 3, the following merit function, $f = f(U(z) - U_i(z, \{p_n\}))^2 dz$ was minimized with respect to the full set of parameters, $\{p_n\}$, for the CG bond lengths, bond (bending) angles, and dihedral angles, respectively: $\{k_b, r_0\}$, $\{k_\theta, \theta_0\}$, and $\{V_1, V_2, V_3, V_4\}$. Using the criterion $|\{p_n\}^i - \{p_n\}^{i-1}| < 10^{-4}$ (i denotes the i th iteration, as for the U_i given above) for each of the parameters belonging to $\{p_n\}$, the total number of iterations

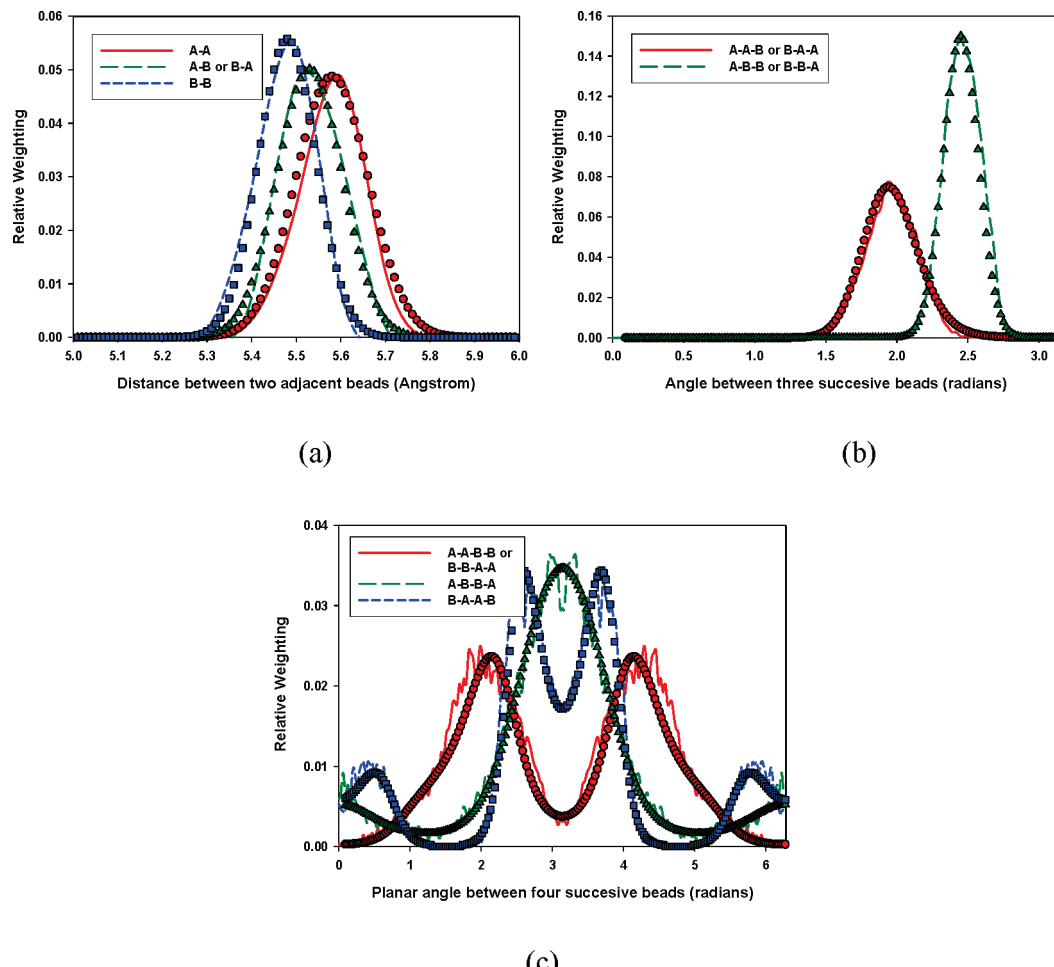


Figure 3. The distribution functions for (a) the bond length, (b) the bond angle, and (c) the planar angle for a 10-mer PANI-EB at 298 K and 1 atm, where AMD and CGMD simulation data are displayed by lines and symbols, respectively.

TABLE 2: Potential Functions Used for the CG Model

intramolecular potentials		notation
bond	$U_{\text{bond}} = \frac{1}{2}k_b(r_{ij} - r_0)^2$	k_b , force constant; r_0 , equilibrium bond length
bond angle	$U_{\text{angle}} = \frac{1}{2}k_\theta[\cos(\theta_{jik}) - \cos(\theta_0)]^2$	k_θ , force constant; θ_0 , equilibrium bond angle
dihedral angle	$U_{\text{dihed}} = \sum_{m=1}^4 V_m[1 + \cos(m\phi_{ijkn})]$	V_m , constants; m , periodicity
intermolecular potentials		
van der Waals	$U_{\text{vdw}} = 4\epsilon[(\sigma/r_{ij})^{12} - (\sigma/r_{ij})^6]$	ϵ, σ : van der Waals parameters

is about 100 for the cases of bond lengths and bond angles and about 500 for the case of dihedral angles. In Figure 3, one sees close agreement between CGMD and AMD simulations for the predicted distributions. Moreover, a single peak in the distribution function for the bending angle (see Figure 3b) has been suggested to better conform to the independence requirement noted above.²⁹ For visualization purposes, a realization of the simulated chain conformation corresponding to the most prob-

able states of the bond lengths and angles shown in Figure 3 has been utilized in Figure 2.

To construct the intermolecular potential for nonbonded beads in the CG polymer model, we utilized the radial distribution functions (RDFs) obtained from AMD simulations for the particle baths, as shown in Figure 4a: $G(r) = n(r)/\rho 4\pi r^2 \Delta r$, where $n(r)$ is the mean number of particles lying within the shell defined by the radial distances r and $r + \Delta r$, respectively.

TABLE 3: Potential Parameters Used for the CG Model

	types	parameters
bond	A–A	$k_b = 71.84 \text{ (kcal mol}^{-1} \text{ \AA}^{-2}\text{)}, r_0 = 5.56 \text{ (\AA)}$
	A–B or B–A	$k_b = 111.28 \text{ (kcal mol}^{-1} \text{ \AA}^{-2}\text{)}, r_0 = 5.52 \text{ (\AA)}$
	B–B	$k_b = 143.03 \text{ (kcal mol}^{-1} \text{ \AA}^{-2}\text{)}, r_0 = 5.47 \text{ (\AA)}$
bond angle	A–A–B or B–A–A	$k_\theta = 19.46 \text{ (kcal mol}^{-1} \text{ rad}^{-2}\text{)}, \theta_0 = 1.94 \text{ (rad)}$
	A–B–B or B–B–A	$k_\theta = 38.80 \text{ (kcal mol}^{-1} \text{ rad}^{-2}\text{)}, \theta_0 = 2.45 \text{ (rad)}$
dihedral angle	A–A–B–B or B–B–A–A	$V_1 = 0.80 \text{ (kcal mol}^{-1}\text{), } V_2 = 0.73 \text{ (kcal mol}^{-1}\text{), }$ $V_3 = -0.03 \text{ (kcal mol}^{-1}\text{), } V_4 = 0.22 \text{ (kcal mol}^{-1}\text{)}$
	A–B–B–A	$V_1 = 0.66 \text{ (kcal mol}^{-1}\text{), } V_2 = -0.54 \text{ (kcal mol}^{-1}\text{), }$ $V_3 = -0.10 \text{ (kcal mol}^{-1}\text{), } V_4 = 0.02 \text{ (kcal mol}^{-1}\text{)}$
	B–A–A–B	$V_1 = 0.45 \text{ (kcal mol}^{-1}\text{), } V_2 = -1.33 \text{ (kcal mol}^{-1}\text{), }$ $V_3 = -0.13 \text{ (kcal mol}^{-1}\text{), } V_4 = 0.67 \text{ (kcal mol}^{-1}\text{)}$
van der Waals	A	$\epsilon_{ii} = 0.32 \text{ (kcal mol}^{-1}\text{), } \sigma_{ii} = 5.14 \text{ (\AA)}$
	B	$\epsilon_{ii} = 0.34 \text{ (kcal mol}^{-1}\text{), } \sigma_{ii} = 5.14 \text{ (\AA)}$
	NMP	$\epsilon_{ii} = 0.30 \text{ (kcal mol}^{-1}\text{), } \sigma_{ii} = 4.95 \text{ (\AA)}$

and ρ is the bulk number density. An iterative procedure was adopted to find the effective two-body potential using the Boltzmann inversion as a first guess.^{20,24} The parameter values are also tabulated in Table 3 for the Lennard-Jones 12–6 potential employed. Again, there is a generally good agreement between the CGMD and AMD simulations for the predicted RDFs. Noticing that the three particle species considered in Figure 4a possess similar RDFs, the cross interactions between two unlike CG particles were described by the same LJ function along with the following mixing rule for the two parameters: $\sigma_{ij} = (\sigma_{ii} + \sigma_{jj})/2$ and $\epsilon_{ij} = (\epsilon_{ii}\epsilon_{jj})^{1/2}$. For a validity check of the above mixing rule, for which controversial results were sometimes noted,^{43,44} the CGMD simulation utilizing the mixing rule has been compared with the original AMD simulation for the bath consisting of an equal amount (500 particles for each species) of A–B, B–NMP, or A–NMP. The results (not shown) have indicated good agreement between these two for the predicted RDFs.

Due to the anisotropic nature of HB and π – π interactions, their effects have been ignored in constructing the mean (isotropic) interaction forces of the spherical CG particles

discussed above. To examine the impact of this essential simplification on the resultant CG polymer model predicting bulk single-chain properties, we have performed a benchmark AMD simulation of a 10-mer PANI-EB in NMP, where HB and π – π interactions were explicitly accounted for in the full-atom polymer model; see additional information in Table 1. Specifically, the AMD simulation utilizes a 10-mer PANI-EB in a bath consisting of 1000 NMP solvent molecules. The chance of forming hydrogen bonds arises from 20 atomic sites of HB donor and 1020 atomic sites of HB acceptor. In addition, the π – π interaction is imposed between any two aromatic rings within the PANI-EB oligomer. The corresponding CG polymer model, as noted above, ignores HB and π – π interactions entirely. Both AMD and CGMD simulations utilize the Nosé–Hoover *NVT* ensemble ($T = 298.15 \text{ K}$ with a coupling constant of 0.1 ps and a density 1.18 g/cm^3) with a time step size of 1 fs for AMD and 2 fs for CGMD. The total simulation time is about 1 ns for both cases, where initial chain equilibration in the AMD simulation has been aided by Monte Carlo simulations.⁴⁰

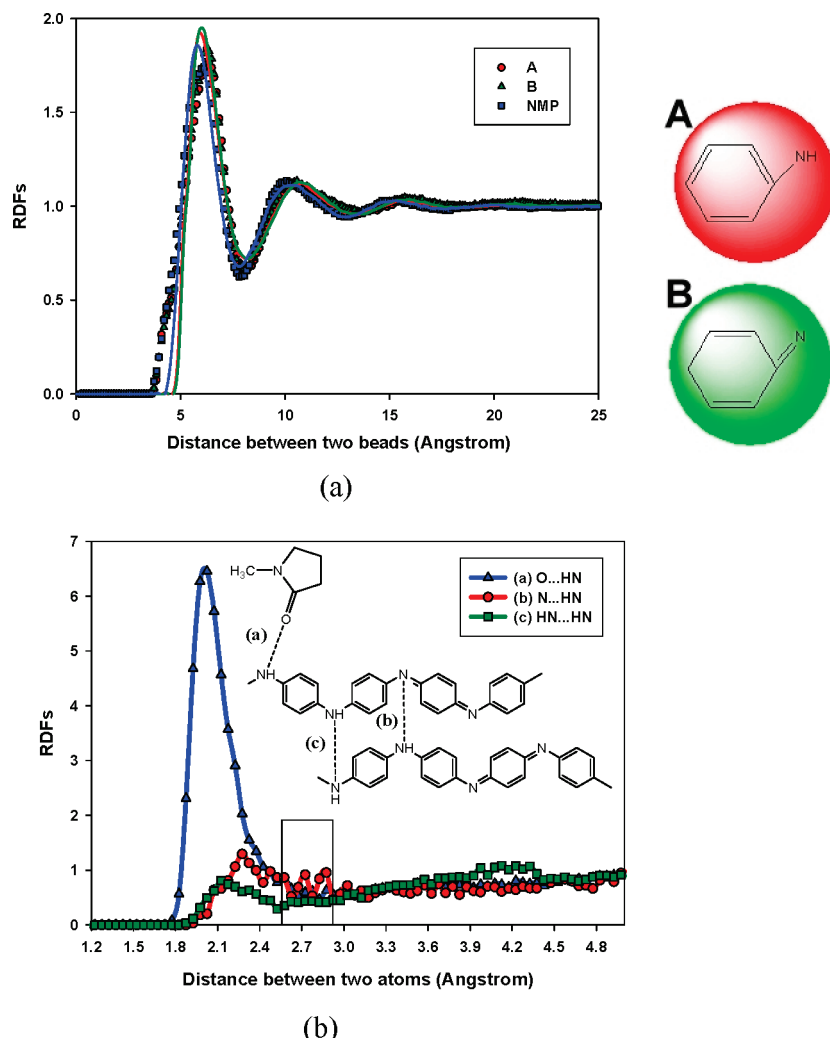


Figure 4. Radial distribution functions (RDFs) at 298 K and 1 atm for (a) the bath of A, B, or NMP, where symbols and lines were from AMD and CGMD simulations, respectively; (b) three potential locations of HB formation for a 10-mer PANI-EB in NMP by AMD simulation, where the expected range for effective HB formation is marked by a rectangular region ($2.75 \pm 0.20 \text{ \AA}$).

TABLE 4: Comparison between the CGMD and AMD (with HB and $\pi-\pi$ Interactions) Simulations for the Predicted Single-Chain Properties in PANI-EB/NMP Solution

method	no. monomer units per chain	no. solvent particles	radius gyration (\AA)	end-to-end distance (\AA)	diffusivity (m^2/s)
AMD	10	1000	14.75 ± 0.27	37.32 ± 1.71	27.92×10^{-10}
CGMD	10	1000	15.68 ± 0.42	41.43 ± 2.83	32.52×10^{-10}

The results compiled in Table 4 indicated that the disparities between AMD and CGMD simulations are systematic, yet are no more significant than simulation error bars. This observation is suggestive of the dominance of segmental vdW interactions in determining bulk single-chain properties in solution. To further confirm this assertion, Figure 4b shows the RDFs for three potential locations of HB formation. Whereas case a represents the solvent–polymer interaction, cases b and c are for intrachain interactions. In the first case, one sees that the peak falls at an interatomic distance notably shorter than the expected one for an effective hydrogen bond, marked by the rectangular region. This observation suggests that the polymer–solvent interactions were dominantly vdW in nature. Similarly, it is clear for the other two cases that the RDFs displayed no significant signature of forming hydrogen bonds, and the entire distributions were controlled by the short-range excluded volume (which is again vdW in nature) as well as by the chain rigidity.

The reasons that the single-chain properties of PANI-EB in solution seem to be little affected by HB and $\pi-\pi$ interactions have an important general implication and may be attributed to the dual effects of chain rigidity of PANI-EB and thermal agitations of the solvent molecules. Noticing that the formation of an effective HB or $\pi-\pi$ bond is extremely sensitive to the relative alignment of the two molecules involved, thermal agitations of the solvent molecules make it difficult for them to form hydrogen bonds with the polymer molecule, as evidenced by Figure 4b. On the other hand, solvent agitations substantially swell the polymer coil and thus greatly reduce the chance of forming intrachain hydrogen bonds. Along with the effect of intrinsic chain rigidity, intrachain hydrogen bonding becomes rare in dilute solution of a typical semiflexible conjugated polymer such as PANI-EB. Note, in addition, that chain rigidity would greatly enhance the influence of segmental vdW interactions, such as the case with rodlike molecules, leading to generally poor solvent qualities for conducting conjugated

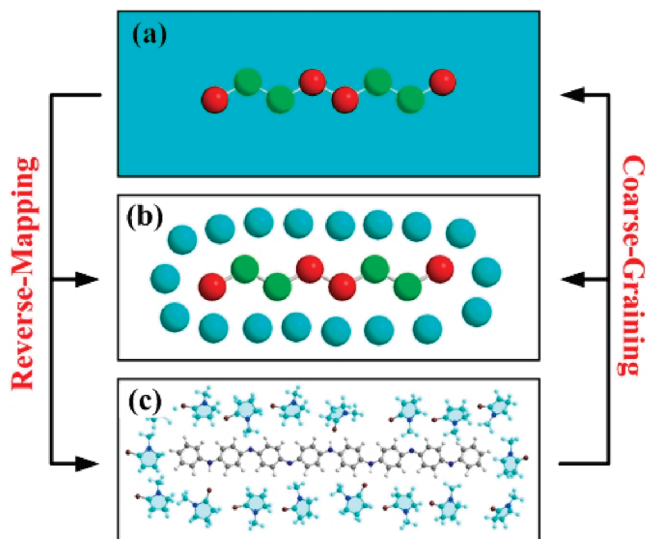


Figure 5. Sketches illustrating (from top to bottom) CGLD, CGMD, and AMD realizations of a 10-mer PANI-EB in NMP; the actual number of solvent molecules used was 1000.

polymers in solution.³⁷ In summary, it appears plausible to conclude that, for a standard conducting conjugated polymer such as PANI-EB, a semiflexible chain backbone along with the effects of solvent agitations have, under typical conditions, made segmental vdW interactions the dominant molecular interactions in controlling single-chain properties in solution. In contrast, for the cases with flexible polymer chains or in a deeply quenched state, anisotropic local interactions may significantly alter the eventual chain conformations, as we demonstrate later for a room-temperature quenching of PANI-EB.

2.3. Construction of CGLD Model. The major conclusions reached in the preceding subsection have motivated the development of a further coarse-grained simulation for PANI-EB solution by replacing the solvent molecules with a self-consistent solvent field. The central idea and procedure have been elucidated in a previous work on a different conjugated polymer without considering HB and $\pi-\pi$ interactions.³⁷ Specifically, we demonstrated how a self-consistent, parameter-free Langevin dynamics (LD) scheme may be constructed for a CG polymer model in specific solvents. Instead of relying on adjustable monomeric frictions, the Einstein relation $D = k_B T / \zeta$ was utilized along with the “measured” monomer diffusivity in an AMD simulation of a solvent bath to obtain a self-consistent frictional coefficient, ζ . The obtained frictional coefficient and fluctuation-dissipation theorem were then employed to construct a self-consistent Langevin dynamics dictating the CG polymer chain, for which the effects of solvent quality on both static and dynamic properties can be well-captured in a computationally very efficient way. The sketches shown in Figure 5 grossly depict the relation between the three simulation models considered in this work. The particle diffusivities of A-mer and B-mer in NMP were found in AMD simulations to be $D_{A,NMP} = 5.2 \times 10^{-9} \text{ m}^2/\text{s}$ and $D_{B,NMP} = 6.4 \times 10^{-9} \text{ m}^2/\text{s}$, respectively, at $T = 298 \text{ K}$ and 1 atm. Accordingly, the Langevin dynamics equation without considering hydrodynamic interactions can be written as

$$m_i \frac{d^2 \mathbf{r}_i}{dt^2} = -\zeta_i \frac{d\mathbf{r}_i}{dt} + \sum_j \mathbf{F}_{ij} + \xi_i \quad (1)$$

where m_i and \mathbf{r}_i are the mass and positional vector of the i th bead on a certain polymer chain, respectively; $\sum_j \mathbf{F}_{ij}$ and ξ_i are the sum of the conservative forces (i.e., the intra- and intermolecular forces) and the random force, respectively, acting on the same bead; and ζ_i is the frictional drag coefficient described above. Note that eq 1 automatically maintains the system temperature, and it may be integrated using an algorithm detailed in ref 39.

In summary, when localized interaction forces were noted to play minor roles for the polymer system and material properties under consideration, similar CGMD or CGLD simulations as introduced above are recommended to gain practical access to long-chain properties that are otherwise difficult to evaluate in experiments or AMD simulations. Several such cases with the PANI-EB solution are demonstrated in the next section. On the other hand, when the effects of HB or $\pi-\pi$ interactions are expected to be crucial, such as in a dense or condensed system, the proposed CG scheme may as well assist searching for representative “precursor” chain realizations that would greatly facilitate the later study with an explicit account of these interaction forces. A subsequent section discussing the quenching morphologies of PANI-EB is devoted to this purpose.

3. Fundamental Single-Chain Properties in Solution by CG Simulations

With the CG models introduced in the preceding section, it is possible to simulate PANI-EB in solution with a chain length as typically studied in real experiment (e.g., 100 monomers per chain or $M_n = 36\,000$). A larger time step size (5 fs) can be used, and accessible real times can be extended to 10–100 ns and even longer on a single-CPU personal computer. Recall that, due to the effect of molecular grouping, the CG time scale typically does not match the real one and, hence, must be properly rescaled through fits with the AMD data on relevant dynamic properties.^{24,37}

First, we evaluate the persistence length which, in general, tells the flexibility of a chain molecule and, in particular, has a major influence on the effective conjugation length of a conducting polymer. The following formula was employed in the CGMD simulation:⁴⁷

$$L_p = \sum_{k \geq j} \langle \mathbf{Q}_j \cdot \mathbf{Q}_k / a \rangle \quad (2)$$

where \mathbf{Q} and a are the bond vector and the average bond length, respectively, and the indices j, k sum over all segments of the same chain. The persistence length was thus estimated to be $L_p = 18.8 \pm 2.1 \text{ \AA}$, which amounts to about two to three PANI-EB repeating units. Comparing this value with the known ones for two flexible polymers (i.e., polyethylene (4.7 Å)⁴⁸ and polystyrene (9.2 Å)⁴⁹) and a widely studied conjugated polymer poly(2-methoxy-5-(2'-ethylhexyloxy)-1,4-phenylenevinylene) (MEH-PPV) (70 Å),³⁷ the moderate rigidity associated with a PANI-EB chain should be evident. Note that, compared to MEH-PPV, the apparent chain flexibility of PANI-EB arises from the nonconjugated amine nitrogen groups.

In principle, one may proceed to geometric properties such as mean radius of gyration and end-to-end distance that yield important knowledge about the exact solvent quality for a specific solvent and system temperature. Dynamic properties, such as center-of-mass diffusivity, can also be evaluated to study the structural compactness of the polymer coil. We note, however, that applying CGMD simulations to a polymer solution

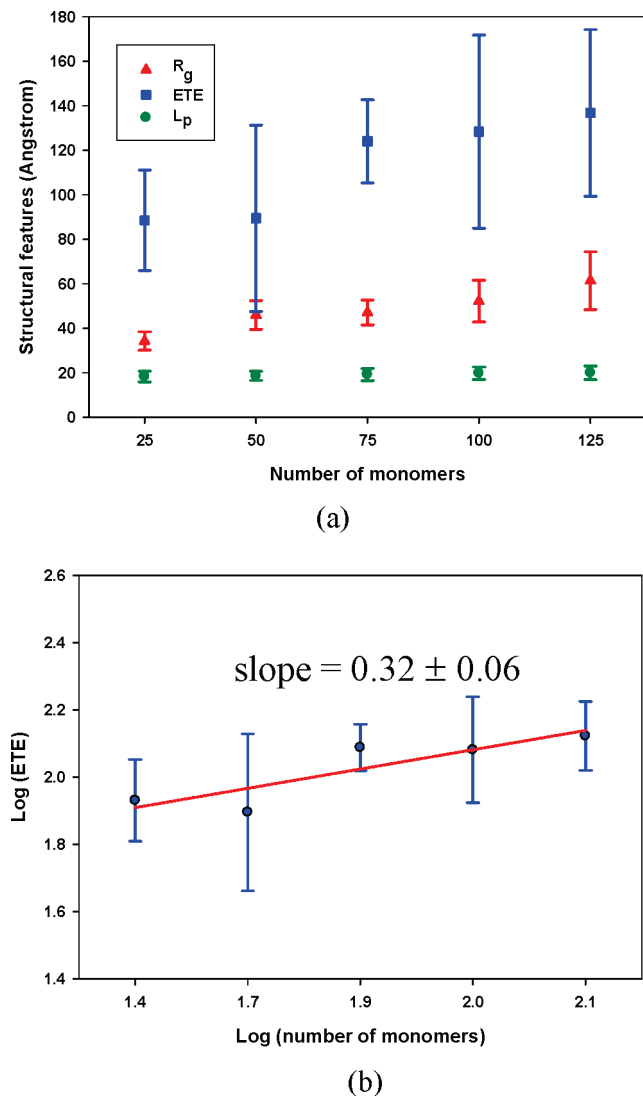


Figure 6. (a) The predicted persistence length (L_p), mean end-to-end distance (ETE), and radius of gyration (R_g) for a single PANI-EB chain in NMP as functions of chain length (plotted in number of monomers); (b) the scaling law of the mean end-to-end distance, which yields a solvent quality exponent of ~ 0.32 .

system is often impractical, especially when explicit solvent molecules that cost most of the computational effort are not a critical concern for the material properties of interest. Possible situations that might, however, demand explicit solvents in a CG simulation include investigations aimed at resolving the precise dynamics of complex structural formation,^{15,16} the dynamics and structures within a compact aggregate cluster, or viscometric properties sensitive to hydrodynamic interactions. Therefore, CGLD simulations were exploited in the following discussion on several fundamental long-chain properties in solution. For comparison, we note that the persistence length of PANI-EB in NMP was estimated to be $L_p = 19.2 \pm 2.7 \text{ \AA}$ by a CGLD simulation, in good agreement with the result given earlier for a CGMD simulation. A general comparison between CGLD and CGMD simulations may be found in an earlier work.³⁷

Figure 6 plots the mean radius of gyration and end-to-end distance as functions of chain length obtained from CGLD simulations. The results shown are valuable for evaluating the solvent quality of PANI-EB/NMP solution, which is difficult to assess using typical experimental protocols or with ordinary AMD or CGMD simulations. The solvent quality exponent was

thus estimated to be 0.32 ± 0.06 , which falls substantially below the so-called θ condition, 0.5, and is comparable to that of MEH-PPV in toluene, a relatively poor solvent for MEH-PPV.³⁷ It is worth noting that the estimated solvent quality exponent, ~ 0.32 , is close to the critical value, 1/3, above which the solvent quality is good enough to ensure a diminishing segmental density within an isolated chain with increasing chain length.⁵⁰ Thus, it is implied that the local segmental density of isolated PANI-EB chains in NMP might keep growing with increasing polymer molecular weight, and chain collapse could result for sufficiently long PANI-EB chains, even at large dilution.

A solvent quality as poor as explored above for PANI-EB/NMP solution is, in fact, expected to be accompanied by the prevalence of interchain aggregates. As a preliminary observation, Figure 7 shows the structural evolution of five initially separated PANI-EB chains. The PANI-EB chains were noted to quickly coalesce into a compact aggregate cluster under the sole influence of vdW forces. Recall, however, that the supramolecular aggregation structures of PANI-EB may differ substantially from the ones seen here, because the CGLD simulation has omitted the influences of HB and $\pi-\pi$ interactions. Nevertheless, at some later stage for the case considered in Figure 7, a systematic back-mapping procedure may be adopted to return the system to full-atom coordinates, at which HB and $\pi-\pi$ interactions may be incorporated and their effects examined in a relatively efficient manner. No related simulation results were shown because the computational effort required is still beyond the reach of the present AMD simulation, although it is, indeed, possible to simulate the aggregation properties for considerably shorter chains. Overall, the simulation suggests that, in contrast with the prevailing conjecture overemphasizing the effects of HB interactions, segmental vdW interactions were identified to be the principal reason to account for the notorious difficulty in dissolving PANI-EB chains in essentially all types of solvents, as well as for the prevalence of interchain aggregates and even gel in solution.

In addition to the structural properties investigated above, single-chain dynamics is usually of interest in, say, a dynamic light scattering experiment, which measures the autocorrelation of scattered light intensities and thus estimates the apparent diffusivity, D_c , of the probed macromolecular species. Usually, the Einstein–Stokes relation is employed to link the apparent chain diffusivity with the so-called hydrodynamic radius, R_h . Moreover, the value of hydrodynamic radius may be compared with the radius of gyration, R_g , determined in static light-scattering measurements so as to infer the structural compactness of the polymer coil in solution. In the literature, the ratios of R_g/R_h have been systematically correlated with the structural compactness of single polymer chains or their aggregates,⁵¹ and a small value of this ratio (roughly < 1) is suggestive of a compact coil structure. Table 5 compares the predicted values of R_h and R_g as well as their ratios for various chain lengths. It is of interest to note that the ratio falls around a fixed value of 1.7 only for chain lengths above 100 repeating units, and the predicted ratio for R_g/R_h (> 1) is indicative of a moderate structural compactness. On the other hand, the disparity between R_h and R_g is quite significant for shorter chains. We noticed, however, that such a conflict has captured little attention in typical dynamic light scattering experiments on polymer solutions. In this way, the simulation provides a definite lower bound in polymer molecular weight ($\sim 36\,000 \text{ Da}$) when dynamic light scattering data will be employed to infer the geometric coil size.

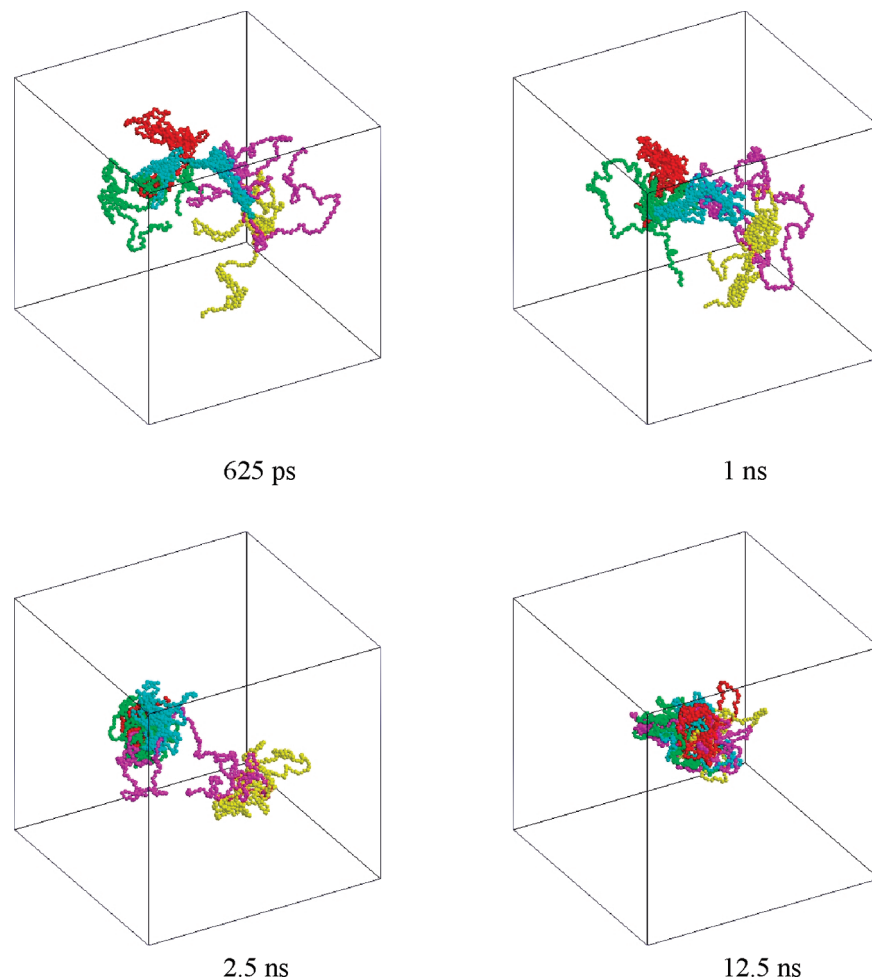


Figure 7. Snapshots illustrating the formation of an aggregate cluster made of five 100-mer PANI-EB in NMP at $T = 298$ K.

TABLE 5: CGLD Simulation Results of the Structural and Dynamic Properties of Single PANI-EB Chains in NMP with Various Chain Lengths

no. monomers per chain	25	50	75	100	125
R_g (\AA)	34.22	45.96	47.10	52.17	61.37
D_c ($\times 10^{-10} \text{ m}^2/\text{s}$)	16.00	8.40	0.93	0.44	0.37
R_h (\AA) ^a	0.83	1.57	14.34	30.05	35.73
R_g/R_h	41.23	29.27	3.28	1.74	1.72

^a Using the Einstein–Stokes relation: $D_c = k_B T / 6\pi R_h \eta_s$ or $R_h = k_B T / 6\pi D_c \eta_s$, where the solvent viscosity for NMP is $\eta_s = 1.65$ cP.

4. Quenched Single-Chain Morphologies

One of the primary objectives of this study is to be able to scrutinize the quenched chain morphologies mimicking the thin-film state, where localized interaction forces are expected to play an important role. The previously explored, dominant effects of vdW interactions in PANI-EB solution as well as the capability of the CGLD simulation to gain practical access to representative long-chain conformations make this mission feasible. First, Figure 8 illustrates the back-mapping procedure that returns an equilibrated PANI-EB chain in NMP from the CGLD simulation (stage a) all the way to the full-atom

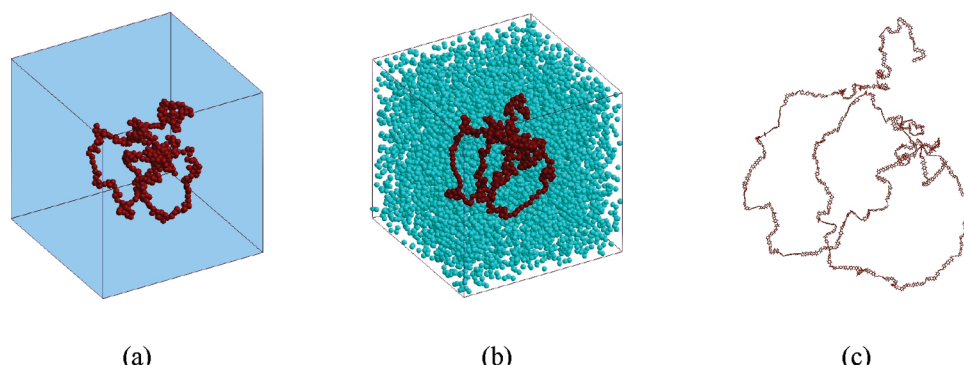


Figure 8. Back-mapping of single-chain realizations for a 100-mer PANI-EB in NMP (400 in total) from (a) CGLD simulation (vdW interactions only; CG simulation time 200 ns) to (b) CGMD simulation (vdW interactions only; NPT ensemble at 1 atm, 298 K; box size = 109.3 \AA ; density = 1.01 g/cm^3 ; and CG simulation time = 10 ns) and (c) AMD simulation (vdW plus HB and $\pi-\pi$ forces; NPT ensemble at 1 atm, 298 K; box size = 108.9 \AA ; density = 1.02 g/cm^3 ; and real time ~ 1 ns).

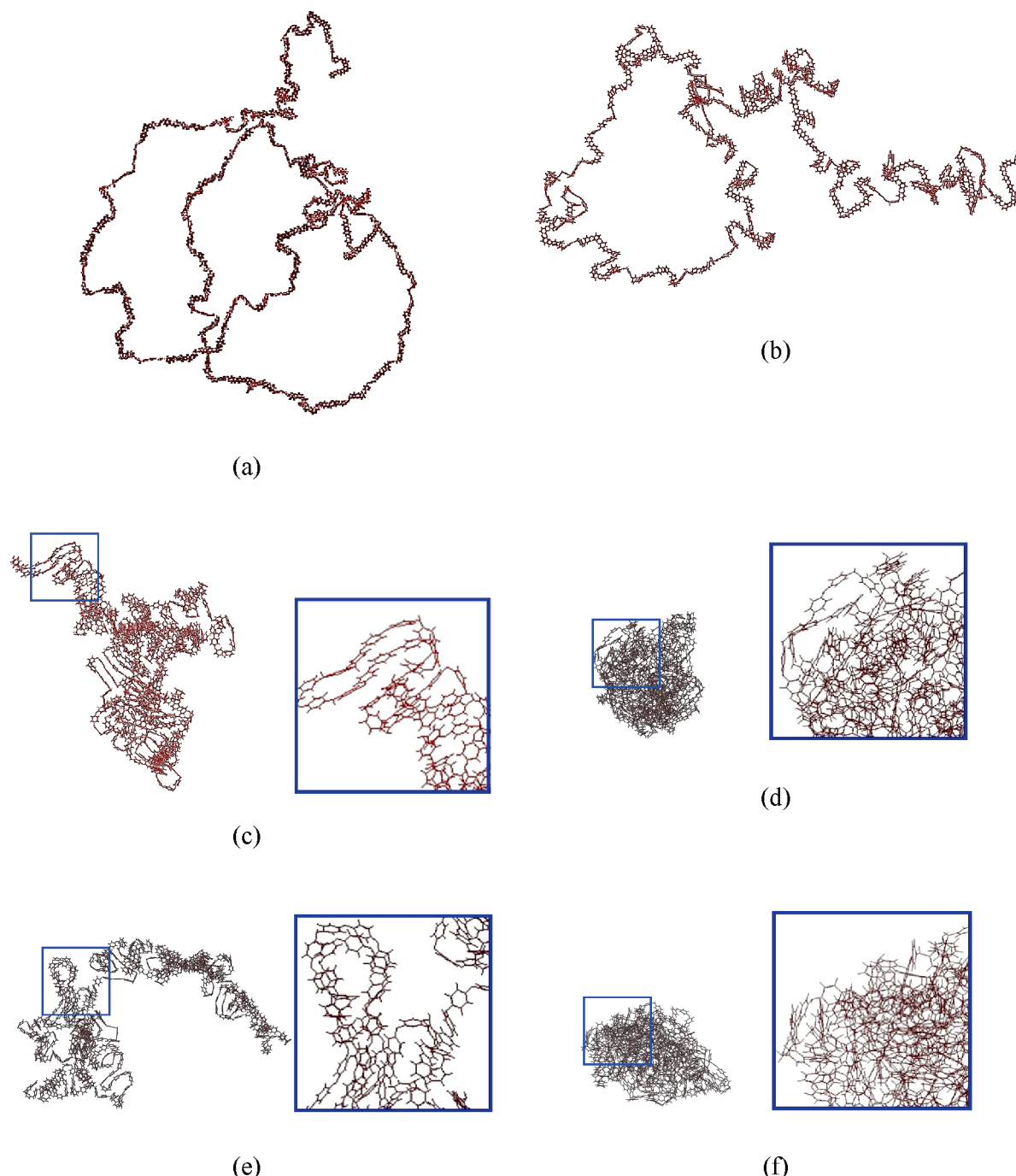


Figure 9. (a–b) Single-chain conformations of a 100-mer PANI-EB in NMP obtained via the reverse mapping as explained in Figure 8; Parts c–f represent the quenching conformations upon instant solvent evacuation of cases a and b, respectively. Whereas the results for parts c and e were obtained by AMD simulations with vdW, HB, and $\pi-\pi$ interactions (*NVT* ensemble at 298 K; box size = 108.9 Å; real time \sim 2 ns), the results for parts d and f considered only vdW interactions.

representation ready for an AMD simulation (stage c). The detailed procedure of back-mapping from CGMD to AMD simulations basically follows those described in the literature.^{17,22,29,31,33,36,38} Upon an instant evacuation of solvent molecules during stage c, when local chain conformations had been further equilibrated in the AMD simulation for about 1 ns, HB and $\pi-\pi$ interactions were selectively turned on or off to discriminate their effects on the collapsed chain morphologies in a room-temperature quenching process.

Two representative cases are examined in Figure 9. These two cases start from two different chain conformations obtained in a way as explained in Figure 8. To gain basic insights, it is assumed that the solvent is removed instantaneously. In practice,

the quenching is often achieved via a more complicated spin-coating or inkjet printing process at a constant temperature, where gradual solvent evaporation is usually accompanied by a complex flow pattern. It is significant to note that, despite the unimportance of localized HB and $\pi-\pi$ interactions in determining bulk single-chain properties in solution, their impact on the quenched chain morphology appears to be enormous. Precisely, these two intermolecular forces play the role of “trapping” a collapsing chain to the observed morphologies, shown in Figure 9c and e, thereby inhibiting the formation of an even more compact, mutually similar, structure under the sole influence of vdW interactions, shown in Figures 9d and f. Locally, the trapping of chain conformation by HB and $\pi-\pi$

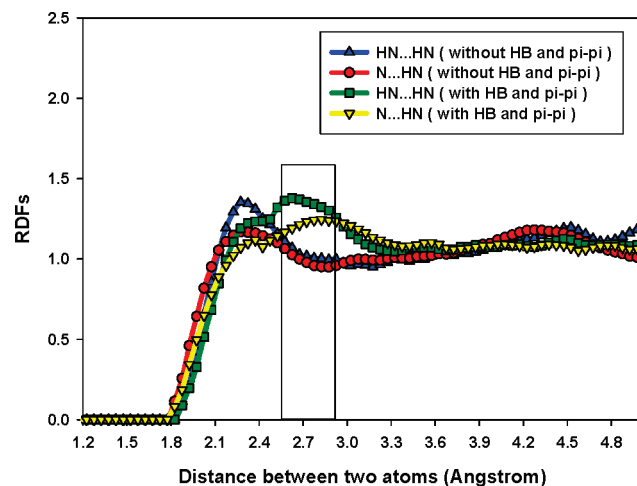


Figure 10. The RDFs for the quenched chain conformations shown in Figure 9, where the expected range for effective HB formation is marked by a rectangular region ($2.75 \pm 0.20 \text{ \AA}$).

interactions can best be perceived by examining the zoomed pictures shown in the same figure. The contrast noted between the cases with or without anisotropic forces is significant. From a different perspective, the signature of forming hydrogen bonds in the quenching state can be easily identified in the corresponding RDF plots shown in Figure 10.

Overall, it appears that, whereas the vdW forces regulate the bulk single-chain properties in PANI-EB/NMP solution, the HB and $\pi-\pi$ interactions accordingly dictate the quenched chain morphologies that mimic closely those in the prior solution state. This central implication is important in practical applications with conducting conjugated polymers, suggesting that the material properties of a collapsed polymer thin film would be notably affected by the molecular states in precursor solution that, in turn, may be systematically controlled by the choices of solvent, polymer concentration, and processing rate. In fact, it has often been surmised that the thin-film properties of a conjugated polymer may, to a large extent, be controlled at the final stage of film collapsing or with some after-treatment such as thermal annealing on the dried film. The simulation results shown in Figure 9, however, provide strong evidence of the so-called memory effect,⁸ emphasizing the importance of controlling the molecular state at the early stage of preparing a precursor solution for the fabrication of a PLED.

In summary, we have demonstrated how the quenching morphologies in a dried thin film that concern high-molecular-weight conducting conjugated polymers may become practically accessible by taking advantage of a multiscale scheme that utilizes a systematic mapping and back-mapping between AMD and CGLD simulations. In many cases, stage b in Figure 8 might be skipped without losing the central information, and the mapping and back-mapping between AMD and CGLD would then become more transparent and efficient. In addition, the quenched chain morphologies reached in Figure 9c and e may further be utilized in first-principles computations to resolve the optoelectronic properties of practical relevance to conducting conjugated polymers^{52,53} or organic pigments.⁵⁴ A possible restriction of this multiphase simulation scheme for usual polymer species may be expected, however, with systems in which internal HB or $\pi-\pi$ bonds have a notable impact on the single-chain conformation in solution, as might be with the cases of relatively flexible chains or low system temperatures.

5. Conclusions

We introduced a multiscale scheme, especially versatile for applications with conducting conjugated polymers and, possibly, other long-chain molecules with similar molecular features, that allows one to circumvent the current difficulty to compromise reaching representative long-chain conformations in solution and, on the other hand, capturing the detailed structures in solution or after quenching. PANI-EB was considered as a practical example to demonstrate how a systematic mapping and back-mapping from AMD, CGMD, to CGLD may be carried out to gain critical insights into fundamental single-chain properties in solution and, furthermore, explore their impact on the quenched chain morphologies in thin film. Thus, the simulation evidenced, for the first time, the so-called memory effect, stressing the intimate correlation between the quenched chain morphology and the prior chain conformation in precursor solution.⁸ Although corresponding aggregation structures remain inaccessible at the present stage, we expect a trend similar to that has been revealed for single chains. Overall, the proposed multiscale scheme and the essential features disclosed for PANI-EB are asserted to apply to typical conducting conjugated polymers that possess, ubiquitously, a semiflexible backbone and localized interaction forces. In addition, the single-chain or aggregate realizations so obtained may further be utilized in first-principles computations to help resolve the optoelectronic properties in solution or in film.^{52,53}

Acknowledgment. This work is supported by the MOE Program for Promoting Academic Excellence of Universities under the Grant no. 96-2752-E-007-006-PAE. The resource provided by the National Center for High-Performance Computing of the ROC is gratefully acknowledged.

References and Notes

- (1) MacDiarmid, A. G. *Angew. Chem., Int. Ed.* **2001**, *40*, 2581.
- (2) Gettinger, C. L.; Heeger, A. J.; Pine, D. J.; Cao, Y. *Synth. Met.* **1995**, *74*, 81.
- (3) Lee, H. M.; Lee, T. W.; Park, O. O.; Zyung, T. *Adv. Mater. Opt. Electron.* **2000**, *10*, 17.
- (4) Angelopoulos, M.; Asturias, G. E.; Ermer, E.; Ray, S. P.; Scherr, E.; MacDiarmid, A. G. *Mol. Cryst. Liq. Cryst.* **1988**, *160*, 151.
- (5) Zheng, W.; Angelopoulos, M.; Epstein, A. J.; MacDiarmid, A. G. *Macromolecules* **1997**, *30*, 2953.
- (6) Yang, D.; Zuccarello, G.; Mattes, B. R. *Macromolecules* **2002**, *35*, 5304.
- (7) Avlyanov, J. K.; Min, Y.; MacDiarmid, A. G.; Epstein, A. J. *Synth. Met.* **1995**, *72*, 65.
- (8) Nguyen, T. Q.; Doan, V.; Schwartz, B. J. *J. Chem. Phys.* **1999**, *110*, 4068.
- (9) Ivanov, V. A.; Paul, W.; Binder, K. *J. Chem. Phys.* **1998**, *109*, 5659.
- (10) Stukan, M. R.; Ivanov, V. A.; Grosberg, A. Yu.; Paul, W.; Binder, K. *J. Chem. Phys.* **2003**, *118*, 3392.
- (11) Schnurr, B.; MacKintosh, F. C.; Williams, D. R. M. *Europhys. Lett.* **2000**, *51*, 279.
- (12) Schnurr, B.; Gittes, F.; MacKintosh, F. C. *Phys. Rev. E* **2002**, *65*, 061904.
- (13) Cooke, I. R.; Williams, D. R. M. *Physica A* **2004**, *339*, 25.
- (14) Montesi, A.; Pasquali, M.; MacKintosh, F. C. *Phys. Rev. E* **2004**, *69*, 021916.
- (15) Liu, C.; Muthukumar, M. *J. Chem. Phys.* **1998**, *109*, 2536.
- (16) Chang, R.; Yethiraj, A. *J. Chem. Phys.* **2001**, *114*, 7688.
- (17) Tschöp, W.; Kremer, K.; Batoulis, J.; Bürger, T.; Hahn, O. *Acta Polym.* **1998**, *49*, 61.
- (18) Shelley, J. C.; Shelley, M. Y.; Reeder, R. C.; Bandyopadhyay, S.; Klein, M. L. *J. Phys. Chem. B* **2001**, *105*, 4464.
- (19) Fukunaga, H.; Takimoto, J. I.; Doi, M. *J. Chem. Phys.* **2002**, *116*, 8183.
- (20) Reith, D.; Pütz, M.; Müller-Plathe, F. *J. Comput. Chem.* **2003**, *24*, 1624.
- (21) Marrink, S. J.; de Vries, A. H.; Mark, A. E. *J. Phys. Chem. B* **2004**, *108*, 750.

- (22) Clancy, T. C. *Polymer* **2004**, *45*, 7001.
- (23) Reith, D.; Meyer, H.; Müller-Plathe, F. *Macromolecules* **2001**, *34*, 2335.
- (24) Faller, R. *Polymer* **2004**, *45*, 3869.
- (25) Faller, R.; Reith, D. *Macromolecules* **2003**, *36*, 5406.
- (26) Boek, E. S.; Padding, J. T.; den Otter, W. K.; Briels, W. J. *J. Phys. Chem. B* **2005**, *109*, 19851.
- (27) Li, X.; Ma, X.; Huang, L.; Liang, H. *Polymer* **2005**, *46*, 6507.
- (28) Shih, A. Y.; Arkhipov, A.; Freddolino, P. L.; Schulten, K. *J. Phys. Chem. B* **2006**, *110*, 3674.
- (29) Harmandaris, V. A.; Adhikari, N. P.; van der Vegt, N. F. A.; Kremer, K. *Macromolecules* **2006**, *39*, 6708.
- (30) Li, X.; Kou, D.; Rao, S.; Liang, H. *J. Chem. Phys.* **2006**, *124*, 204909.
- (31) Spyriouni, T.; Tzoumanekas, C.; Theodorou, D.; Müller-Plathe, F.; Milano, G. *Macromolecules* **2007**, *40*, 3876.
- (32) Carbone, P.; Negri, F.; Müller-Plathe, F. *Macromolecules* **2007**, *40*, 7044.
- (33) Santangelo, G.; Matteo, A. D.; Müller-Plathe, F.; Milano, G. *J. Phys. Chem. B* **2007**, *111*, 2765.
- (34) Noid, W. G.; Liu, P.; Wang, Y.; Chu, J. W.; Ayton, G. S.; Izvekov, S.; Andersen, H. C.; Voth, G. A. *J. Chem. Phys.* **2008**, *128*, 244115.
- (35) Noid, W. G.; Chu, J. W.; Ayton, G. S.; Krishna, V.; Izvekov, S.; Voth, G. A.; Das, A.; Andersen, H. C. *J. Chem. Phys.* **2008**, *128*, 244114.
- (36) Karimi-Varzaneh, H. A.; Carbone, P.; Müller-Plathe, F. *J. Chem. Phys.* **2008**, *129*, 154904.
- (37) Lee, C. K.; Hua, C. C.; Chen, S. A. *J. Phys. Chem. B* **2008**, *112*, 11479.
- (38) Peter, C.; Site, L. D.; Kremer, K. *Soft Matter* **2008**, *4*, 859.
- (39) Allen, M. P.; Tildesley, D. J. *Computer Simulations of Liquids*; Clarendon: Oxford, 1990.
- (40) Landau, D. P.; Binder, K. A. *Guide to Monte Carlo Simulations in Statistical Physics*; Cambridge: New York, 2001. The initial chain configuration within the atomistic model was created by a commercial software package, ChemOffice [<http://www.cambridgesoft.com/software/ChemOffice/>], and the number of Monte Carlo steps executed was set to be $\sim 10^3$ – 10^4 times the total number of atoms or beads to ensure that the variations in total energy and end-to-end distance were within 10%.
- (41) Smith, W.; Forester, T. R. *The DL_POLY_2 Reference Manual*; Laboratory Daresbury: Daresbury; 2001.
- (42) Mayo, S. L.; Olafson, B. D.; Goddard, W. A. *J. Phys. Chem.* **1990**, *94*, 8897.
- (43) Sun, Q.; Pon, F. R.; Faller, R. *Fluid Phase Equilib.* **2007**, *261*, 35.
- (44) Carbone, P.; Varzaneh, H. A. K.; Chen, X.; Muller-Plathe, F. *J. Chem. Phys.* **2008**, *128*, 064904.
- (45) Pimentel, G. C.; McClellan, A. L. *The Hydrogen Bond*; Freeman: San Francisco, 1960.
- (46) Hunter, C. A.; Sanders, J. K. M. *J. Am. Chem. Soc.* **1990**, *114*, 112.
- (47) Öttinger, H. C. *J. Non-Newtonian Fluid Mech.* **2004**, *120*, 207.
- (48) Banaszak, B. J.; de Pablo, J. J. *J. J. Chem. Phys.* **2003**, *119*, 2456.
- (49) Brûlet, A.; Boué, F.; Cotton, J. P. *J. Phys. II France* **1996**, *6*, 885.
- (50) Doi, M.; Edwards, S. F. *The Theory of Polymer Dynamics*; Oxford: New York, 1986.
- (51) Zhang, G.; Wu, C. *Adv. Polym. Sci.* **2006**, *195*, 101.
- (52) Sumpter, B. G.; Kumar, P.; Mehta, A.; Barnes, M. D.; Shelton, W. A.; Harrison, R. J. *J. Phys. Chem. B* **2005**, *109*, 7671.
- (53) De Leener, C.; Hennebicq, E.; Sancho-Garcia, J.-C.; Beljonne, D. *J. Phys. Chem. B* **2009**, *113*, 1311.
- (54) Fukunaga, H.; Fedorov, D. G.; Chiba, M.; Nii, K.; Kitaura, K. *J. Phys. Chem. A.* **2008**, *112*, 10887.

JP907338J